ELSEVIER

Chemical Engineering Journal 139 (2008) 208–212

Chemical Engineering Journal

www.elsevier.com/locate/cej

Electrodeposition of maghemite (γ-Fe_2O_3) nanoparticles

Hosik Park [a,b], Perla Ayala [a], Marc A. Deshusses [a], Ashok Mulchandani [a], Heechul Choi [b], Nosang V. Myung [a,*]

[a] *Department of Chemical and Environmental Engineering, University of California-Riverside, Riverside, CA 92521, United States*
[b] *Department of Environmental Science and Engineering, Gwangju Institute of Science and Technology, 1 Oryong-dong, Buk-gu, Gwangju 500-712, Republic of Korea*

Received 9 July 2007; received in revised form 16 October 2007; accepted 22 October 2007

Abstract

Crystalline maghemite (γ-Fe_2O_3) nanoparticles were cathodically electrodeposited at room temperature from environmentally benign electrolytes. The shape, size, and production rate of nanoparticles were strongly influenced by electrochemical conditions (e.g. $FeCl_3$ concentration, current density). X-ray photoelectron spectroscopy (XPS) and X-ray diffraction (XRD) analysis indicated that randomly oriented polycrystalline maghemite nanoparticles were synthesized with the (3 1 1) and (4 4 0) peaks as the main diffraction peaks. Transmission electron microscopy (TEM) images revealed that average particle size decreased from approximately 23 to 7 nm with increased current density. Magnetic saturation (M_S) of maghemite nanoparticles was determined to be 66 emu g^{-1} (66 $Am^2\,kg^{-1}$) at 300 K. The present maghemite nanoparticles showed a greater As(V) adsorption compared to iron nanoparticles, which might be attributed to a higher specific surface area.

Keywords: Electrodeposition; Maghemite; Nanoparticles; Environmental remediation; As(V); Adsorption

1. Introduction

Nanoparticles and one-dimensional nanostructures are the focus of many researchers because they often exhibit unique properties, which cannot be achieved by their bulk counterparts [1–3]. Magnetic nanoparticles are an important class of functional nanomaterials which possess unique magnetic properties. The potential applications of magnetic nanoparticles include ferrofluids for audio speakers [4], surface functionalized probes for biosensors and targeted drug delivery [5], magnetic storage media, powder compacts for power generation, contrasting agents in magnetic resonance imaging and adsorbents for toxic environmental pollutants [6].

Maghemite (γ-Fe_2O_3) is a ferromagnetic oxide that has been widely used as a magnetic recording material for tape drives. In addition, maghemite nanoparticles have been utilized as ferrofluids hyperthermia (MFM) in tumor treatment because of good chemical stability and biocompatibility with high heating capacity in the presence of alternating magnetic fields [6,7].

Various wet chemical processes have been used to synthesize maghemite nanoparticles including precipitation, thermolosis by organic metallic decomposition and carbonyl decomposition [8]. Chemical precipitation is one of the oldest and simple techniques for the synthesis of nanoparticles [8]. In precipitation processes, the metal precursors (e.g. $FeCl_3$ or $FeCl_2$) are dissolved in a solvent and a precipitating agent (e.g. NH_4OH) is added to form nanoparticles. Even though chemical precipitation is simple and manufacturable, this process is difficult to control and yields nanoparticles with a broad size distribution and irregular morphology. Thermolosis can produce monodispersed maghemite nanoparticles with good crystallinity by thermal decomposition of iron cupferron complexes in octylamine and thermal decomposition of iron pentacarbonyl in the presence of oleic acid, respectively [9,10]. Although thermolosis in the presence of capping agents offers monodisperse nanoparticles with good crystallinity, these methods operate at higher temperature (100–300 °C) and require toxic and expensive precursors. These methods have limited controllability of particle morphology and size causing the variation of magnetic properties.

Electrodeposition is a promising alternative technique for fabrication of nanoparticles, because it is simple, manufacturable, inexpensive, fast, operates at near room temperature, and

* Corresponding author. Tel.: +1 951 827 7710; fax: +1 951 827 5696.
E-mail address: myung@engr.ucr.edu (N.V. Myung).

1385-8947/$ – see front matter © 2007 Elsevier B.V. All rights reserved.
doi:10.1016/j.cej.2007.10.025

its ability to control composition, crystallinity, and properties of the deposit by adjusting deposition conditions.

Iron oxide thin films were both cathodically and anodically electrodeposited [11–19]. In the case of anodic formation of iron oxides, the different phases of the iron oxides–oxyhydroxides thin films were obtained by adjusting deposition potentials and solution composition [11]. Zotti et al. [17] reported the cathodic electrodeposition of amorphous Fe_2O_3 thin films by reduction of Fe (III) perchlorate in oxygenated acetonitrile where ferric ions reduced with dissolved oxygen to form amorphous Fe_2O_3. Amorphous Fe_2O_3 thin films were later converted to α-Fe_2O_3 (i.e. hematite) thin films after heat treatment. Schrebler et al. [18] electrodeposited amorphous and nanocrystalline α-Fe_2O_3 (i.e. hematite) thin films from electrolytes containing 5 mM $FeCl_3$ + 1M H_2O_2 + 5 mM KF + 0.1 M KCl at 50 °C. The reduction of hydrogen peroxide at the cathode caused an increase in local pH on the surface of the cathode which later directed the surface precipitation of $Fe(OH)_3$. Ferric hydroxides were later transformed to Fe_2O_3 by the thermal annealing in air. Favier et al. synthesized amorphous maghemite nanoparticles by anodic dissolution of a sacrificial Fe anode, followed by chemical reaction in an organic medium [19].

In this work, we demonstrated a simple method for the electrochemical deposition of crystalline maghemite (γ-Fe_2O_3) nanoparticles by cathodic reaction at room temperature in environmentally benign aqueous electrolytes. In addition, we demonstrate the ability to control the particle size, morphology and production rate by adjusting the deposition conditions. Furthermore, electrodeposited maghemite nanoparticles were applied to remediate As(V) in aqueous solutions.

2. Experimental

2.1. Electrochemical synthesis and characterization

Maghemite nanoparticles were cathodically electrodeposited from electrolytes with various $FeCl_3$ concentrations (i.e. 0.01, 0.05, and 0.10 M of $FeCl_3$) under gavalnostatic control at 20 °C. The electrochemical cell was a 150 ml glass jar with a working volume of 100 ml, an open to the atmosphere. Steel rods served as both the cathode and anode. The surface area of cathode was fixed at 4 cm^2. The pH of solution was adjusted to 2 by adding HCl or NaOH. The current densities were varied from 150 to 2000 mA cm^{-2}. All reagents used in this study were reagent grade. Ultrapure water was used in preparation of solutions (Milli-Q Academic, Millipore). Resistivity of ultrapure water was 18.2 MΩ cm at 25 °C and concentration range of TOC was 5–10 ppb level.

To determine the phase and composition of nanoparticles, X-ray photoelectron spectroscopy (XPS) analysis was performed using a Physical Electronics 5500/5600 ESCA system with monochromatic Al K_α radiation (1486.7 eV) as the X-ray source. The crystal structure of nanoparticles was determined using X-ray diffraction with a Miniflex diffractometer by Rigaku Corp using Cu K_α radiation. The size and morphology of nanoparticles were characterized by transmission electron microscopy (TEM). The magnetic properties of nanoparticles were measured using a magnetic property measurement system (MPMS, Quantum Design) at room temperature with applied magnetic field up to ±4 kOe.

2.2. As(V) remediation

As(V) stock solutions (1000 mg L^{-1}) were prepared using analytical-grade $Na_2HAsO_4{\cdot}7H_2O$ (Sigma Aldrich Chemical Co.) and diluted as needed. 1 M HCl or NaOH solutions were used for pH adjustment. All experiments were performed in 0.01 M NaCl background solution.

As(V) remediation with using maghemite nanoparticles was conducted by reacting 1 mg L^{-1} As (V) in 0.01 M NaCl with varying maghemite nanoparticles concentrations (0.10, 0.5, 0.75, and 1.00 g L^{-1}). For these experiments, maghemite nanoparticles were synthesized at 500 mA cm^{-2} in 0.01 M $FeCl_3$ electrolytes as described in the previous section. At predetermined times, tests tubes in which experiments were conducted were centrifuged, the supernatant was filtered through a 0.22 μm pore PVDF filter, and analyzed by for total arsenic by atomic adsorption spectroscopy (AAS).

3. Results and discussion

Fig. 1 shows the dependence of the production rate on the current density and $FeCl_3$ concentrations. As expected, the production rate linearly increased with increasing current density. The maximum production rate was observed at 0.05 M $FeCl_3$ and as the concentration of $FeCl_3$ was increased to 0.10 M, the production rate decreased might be attribution to the increase in side reactions including ferric ions to ferrous ions and ferrous ions to metallic iron.

Since iron oxide nanoparticles were electrodeposited in naturally aerated solution, two competitive electrochemical reactions may occur at the cathode. Dissolved oxygen can be reduced and then combines with ferric ions to form Fe_2O_3 which is insoluble (Eq. (1)). However, this process is probably limited by dissolved

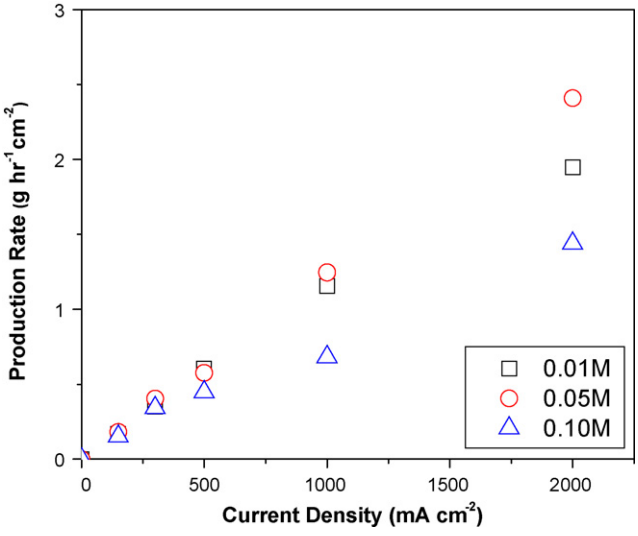

Fig. 1. Dependence of the maghemite nanoparticle production rate on the applied current density and the $FeCl_3$ concentration.

oxygen concentration. Another possible reaction is via hydrogen gas evolution (Eq. (2a)) which may cause an increase in local pH on the surface of cathode. This promotes the formation of ferric hydroxides (Eq. (2b)). Ferric hydroxides later convert to form Fe_2O_3 (Eq. (2c)). The overall reaction is shown in Eq. (2d). It was experimentally observed that there was a significant amount of hydrogen gas evolution during electrodeposition. This and the low dissolved oxygen concentration in solution suggest that Reaction 2 is the dominant electrodeposition reaction pathway to form Fe_2O_3.

Reaction 1

$$4Fe^{3+} + 3O_2 + 12e^- \rightarrow 2Fe_2O_3 \quad (1)$$

Reaction 2

$$6H_2O + 6e^- \rightarrow 3H_2(g) + 6OH^- \quad (2a)$$

$$2Fe^{3+} + 6OH^- \rightarrow 2\,Fe(OH)_3 \quad (2b)$$

$$2Fe(OH)_3 \rightarrow Fe_2O_3 + 3H_2O \quad (2c)$$

$$2Fe^{3+} + 3H_2O + 6e^- \rightarrow Fe_2O_3 + 3\,H_2(g) \quad (2d)$$

XPS spectrums and X-ray diffraction patterns were collected to determine the phase, composition, and crystallinity of iron oxide nanoparticles. Fig. 2 shows the XPS spectrum of iron oxide nanoparticles deposited at 500 mA cm^{-2} in 0.01 M $FeCl_3$. As shown in Fig. 2, the position of the Fe ($2p_{3/2}$) and Fe ($2p_{1/2}$) peaks were at 711.1 and 724.9 eV, respectively, which is similar to bulk counterpart (i.e. Fe ($2p_{3/2}$) at 711 eV and Fe ($2p_{1/2}$) at 725 eV) [20,22]. From the XPS analysis, the atomic ratio of iron and oxygen was also determined to be approximately 2:3, verifying the formation of Fe_2O_3. Unlike bulk hematite, which has two distinct Fe ($2p_{3/2}$) peaks, one narrow Fe ($2p_{3/2}$) peak was observed that matched maghemite [21-23]. In addition, C_1S and O_1S were observed at 285.4 and 530.4 eV, respectively. These results suggested that electrodeposited iron oxide nanoparticles are maghemite.

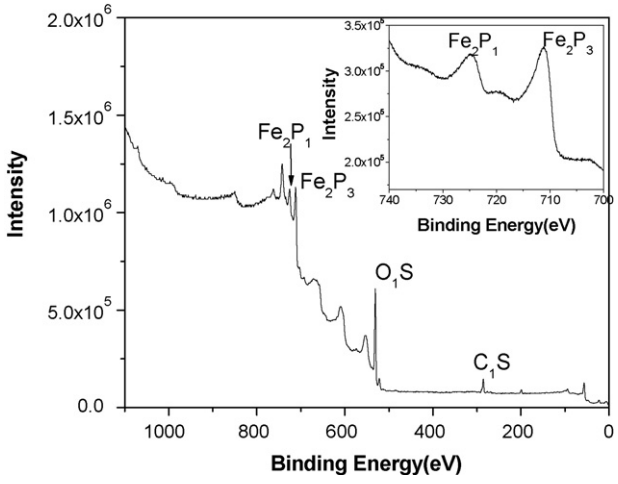

Fig. 2. XPS spectra of the electrodeposited maghemite nanoparticles. Maghemite nanoparticles were synthesized at 500 mA cm^{-2} in 0.01 M $FeCl_3$.

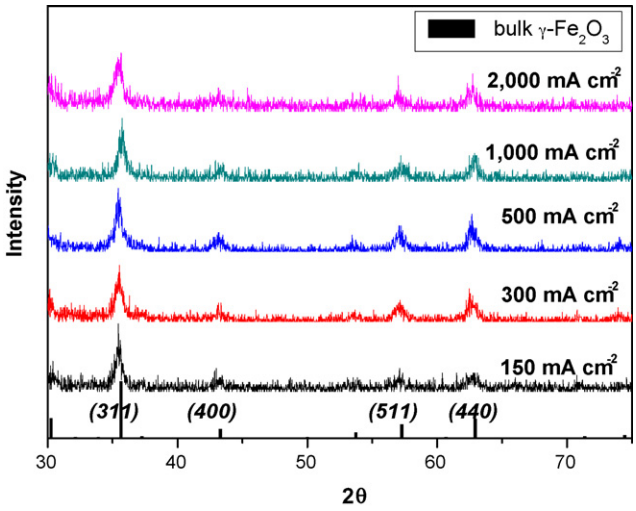

Fig. 3. X-ray diffraction patterns of the maghemite nanoparticles. Maghemite nanoparticles were synthesized at 500 mA cm^{-2} in 0.01 M $FeCl_3$.

Fig. 3 shows the X-ray diffraction patterns of the maghemite nanoparticles prepared at different current densities. Independent of the current density, nanoparticles were randomly oriented polycrystalline with two main diffraction peaks at (3 1 1) and (4 4 0). However, the X-ray diffraction intensity of (3 1 1) and (4 4 0) slightly decreased and increased with increasing current densities, respectively, indicating the slight changes in crystal structure as a function of current density.

Transmission electron microscopy (TEM) was utilized to investigate the shape and size dependence of maghemite nanostructures as functions of current density and electrolyte compositions (Fig. 4). The shape and size of nanoparticles were strongly influenced by electrolyte composition and applied current density. For example, dendritic maghemite nanostructures with approximately 800–1200 nm thick trunks and 50–210 nm thick branches were synthesized at 150 mA cm^{-2} in 0.01 M $FeCl_3$ (Fig. 4a). However, as the concentration and current density increased, spherical shaped nanoparticles were observed (Fig. 4b–i). In all cases, the size of nanoparticles decreased with increased current density (Fig. 5), though this was most pronounced at 0.01 M $FeCl_3$ for which the average size of the nanoparticles decreased from 23 to 7 nm with increasing the current density from 500 to 2000 mA cm^{-2}. The change in morphology and size with the increase in current density might be attributed to the (1) higher nucleation rate; (2) shift reaction control from kinetic control to mass transfer control; and (3) non-uniform electric field cause by nanostructure formation at the electrode surface. At relatively high deposition current density (e.g.150 mA cm^{-2} in 0.01 M $FeCl_3$), the local current density at the electrode is not uniform because of the higher electrical field at the edge of the growing deposit, which favors the nucleation at the tip of the deposit. These conditions can lead to the formation of dendrites. When the deposition current density is very high (e.g. >500 mA cm^{-2}), powdered deposits (i.e. micro or nanoparticles) are formed on the cathode due to the high nucleation rate. The deposit morphology shifts from dendritic to powdery deposits similar to other electrodeposi-

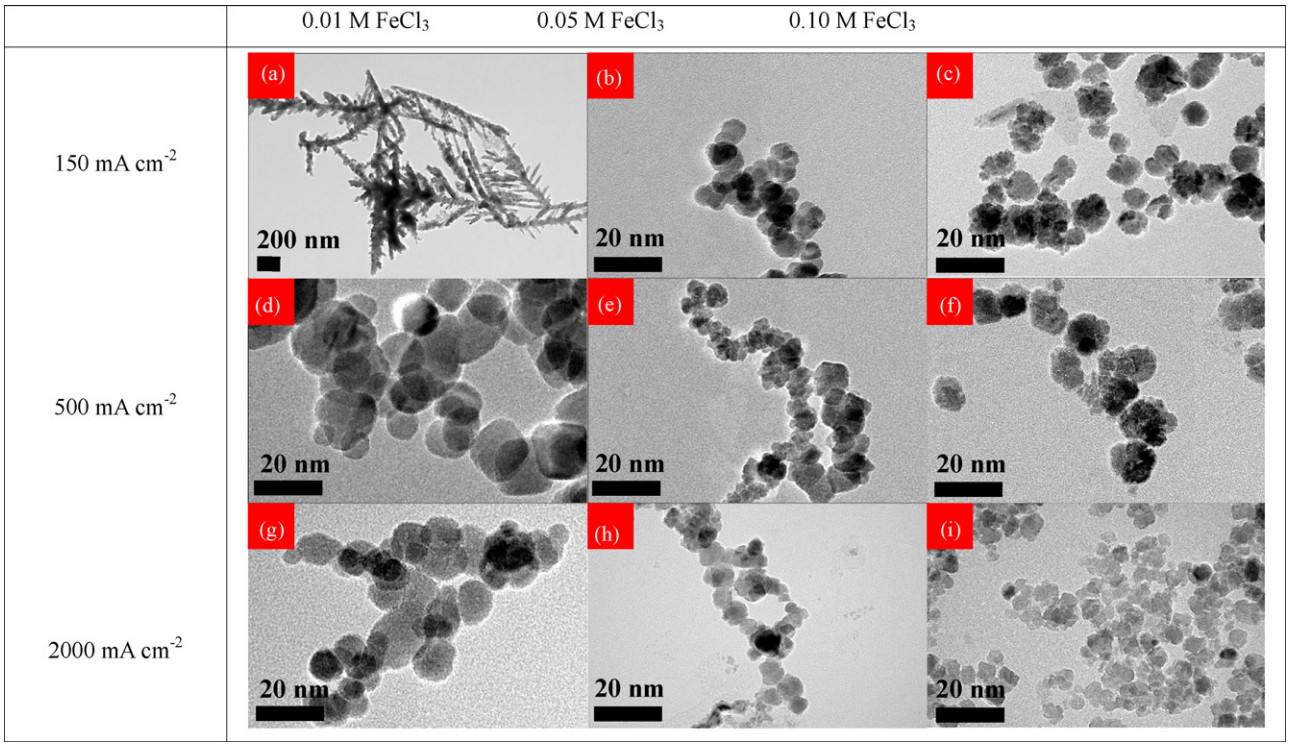

Fig. 4. TEM images of maghemite nanoparticles: current densities were (a–c) 150 mA cm^{-2}; (d–f) 500 mA cm^{-2}; (g–i) 2000 mA cm^{-2}; electrolyte compositions were (a, d, g) 0.01 M $FeCl_3$, (b. e, h) 0.05 M $FeCl_3$, (c, f, i) 0.10 M $FeCl_3$.

tion systems [24]. These results clearly demonstrate that the shape and size of maghemite nanoparticles can be controlled by adjusting electrolyte compositions and deposition current density.

Fig. 6 shows the B-H loop of maghemite nanoparticles at 300 K. The magnetic saturation (M_S) and coercivity (H_C) were determined to be 66 emu g^{-1} ($Am^2\,kg^{-1}$) and 59 Oe (4.7×10^3 A m^{-1}), respectively. Both M_S and H_C were similar to maghemite nanoparticles synthesized by DC thermal arc plasma method and solvothermal reduction method [22,25].

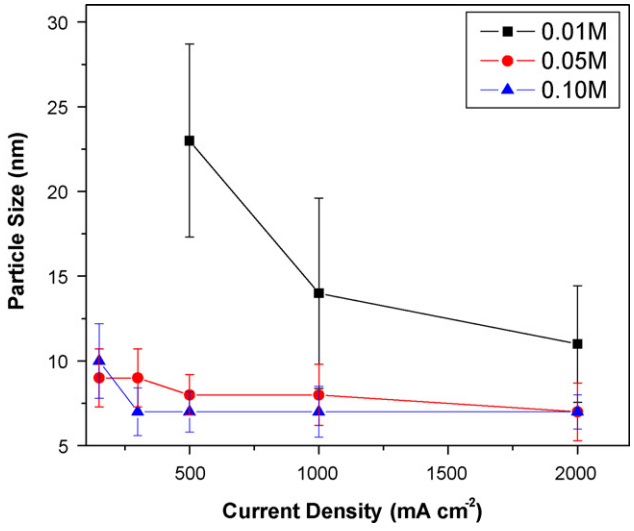

Fig. 5. Average maghemite nanoparticles diameter as a function of the applied current density and the concentration of $FeCl_3$. The error bars show one standard deviation.

Lastly, the adsorption capacity of the nanoparticles was determined using arsenate (As(V)) as a model pollutant. As shown in Fig. 7, As(V) was rapidly removed from solution and reached an equilibrium within 5–20 min of exposure to the maghemite nanoparticles. Arsenic adsorption followed a pseudo first order reaction as follows:

$$\text{Rate} = -\frac{d[As_{tot}]}{dt} = k_{obs}[\gamma\text{-}Fe_2O_3] \quad (3)$$

where $[As_{tot}]$ is the soluble arsenic concentration (mg L^{-1}), [γ-Fe_2O_3] is the concentration of maghemite nanoparticles (g L^{-1}), and k_{obs} is the pseudo first order rate constant (min^{-1}). The

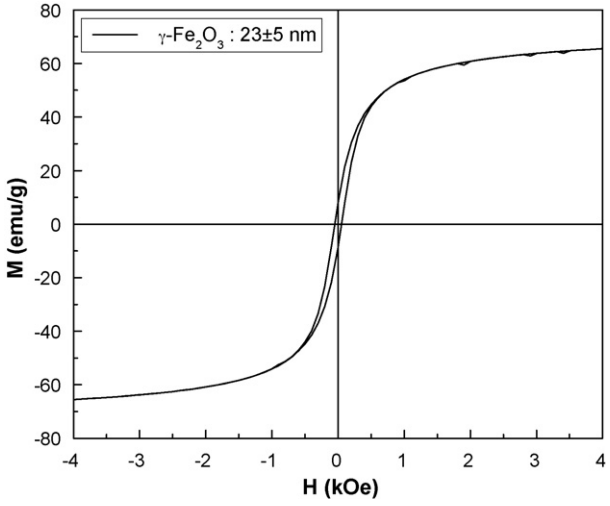

Fig. 6. B-H loop of maghemite nanostructures (500 mA cm^{-2}, 0.01 M $FeCl_3$).

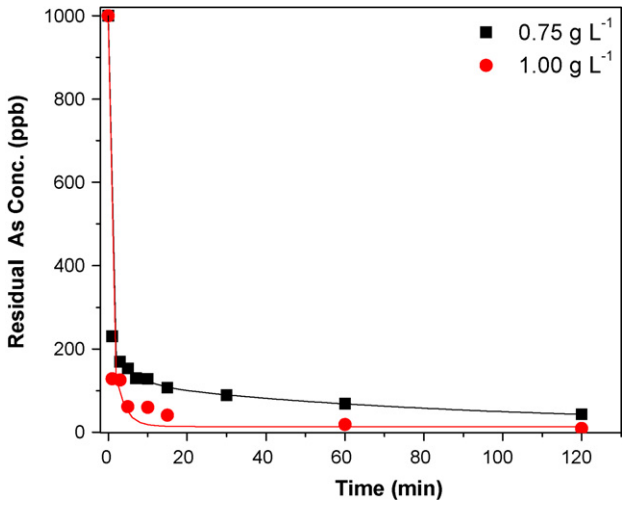

Fig. 7. Experimental data (symbols) and pseudo first-order fitting (lines) of the adsorption of 1 mg L^{-1} As(V) at different maghemite nanoparticle concentration (0.75 and 1.00 g L^{-1}) in 0.01 M NaCl at pH 7.

pseudo first order rate constants (k_{obs}) for As(V) was determined to be 0.11, 0.92, 2.15 and 2.43 min^{-1} at 0.1, 0.5, 0.75 and 1.0 g L^{-1} maghemite nanoparticles, respectively. This is about three times higher compared to zero-valent iron nanoparticles (NZVI) [26]. The specific surface area of maghemite nanoparticles was 41.54 m^2 g^{-1} compare to 25 m^2 g^{-1} for NZVI [26]. This improved reactivity of maghemite nanoparticles compared to the NZVI might be attributed to higher specific surface area. An added advantage of maghemite compared to NZVI is that maghemite is non-reactive and will not reduce As(V) to its more toxic form As(III).

4. Conclusions

Randomly oriented polycrystalline maghemite (γ-Fe_2O_3) nanoparticles were electrodeposited from environmentally benign electrolytes. The morphology and production rate of nanoparticles could be precisely controlled by adjusting the current density and the electrolyte compositions. Transmission electron microscopy (TEM) images showed that size of particle decreased when increasing the current density and the $FeCl_3$ concentration. Maghemite nanoparticles showed a greater adsorption kinetics for As(V) compared to zero valent iron nanoparticles which might be attributed to the higher specific surface area. Compared to other methods, electrodeposition is often a cost effective bulk quantity production method to synthesize nanoparticles with good controllability over size, shape and crystallinity.

Acknowledgement

This work was supported by the Korea Science and Engineering Foundation (KOSEF) grant (no. M10500000-12806J000012810) through the National Research Laboratory Program by the Korea government (MOST) and University of California Toxic Substances Research & Teaching Program (UC TSR & TP).

References

[1] A.P. Alivisatos, Science 271 (1996) 933–937.
[2] R.C. Ashoori, Nature 379 (1996) 413–419.
[3] B.H. Sohn, R.E. Cohen, G.C. Papaefthymiou, J Magn. Magn. Mater. 182 (1998) 216–224.
[4] M.M. Miller, G.A. Prinz, S.F. Cheng, S. Bounnak, Appl. Phys. Lett. 81 (2002) 2211–2213.
[5] S. Sun, C.B. Murray, D. Weller, L. Folks, A. Moser, Science 287 (2000) 1989–1992.
[6] J. Hu, G. Chen, I.M.C. Lo, J. Envron. Eng. 132 (2006) 709–715.
[7] S.-J. Lee, J.-R. Jeong, S.-C. Shin, J.-C. Kim, J.-D. Kim, J Magn. Magn. Mater. 282 (2004) 147–150.
[8] M.A. Willard, L.K. Kurihara, E.E. Carpenter, S. Calvin, V.G. Harris, Inter. Maters. Rev. 49 (2004) 125–170.
[9] D. Chen, R. Xu, J of Solid State Chem. 137 (1998) 185–190.
[10] A. Bee, R. Massart, S. Neveu, J Magn. Magn. Mater. 149 (1995) 6–9.
[11] L. Martinez, D. Leinen, F. Martin, M. Gabas, J.R. Ramos-Barrado, E. Quagliata, E.A. Dalchiele, J. Electrochem. Soc. 154 (2007) D126–D133.
[12] D. Carlier, C. Terrier, C. Arm, J.Ph Anserment, Electrochem. Solid-State Lett. 8 (2005) C43–C46.
[13] T.A. Sorenson, S.A. Morton, G.D. Waddill, J.A. Switzer, J. Am. Chem. Soc. 124 (2002) 7604–7609.
[14] S. Chatman, A.J.G. Noel, K.M. Poduska, J. Appl. Phys. 98 (2005) 113902-1–1113902-6.
[15] L.Y. Zhang, D.S. Xue, X.F. Xu, A.B. Gui, C.X. Gao, J. Phys.; Condens. Matter. 16 (2004) 4541–4548.
[16] M.P. Nikiforov, A. Vertegel, M.G. Shumsky, J.A. Switzer, Adv. Maters. 12 (2000) 1351–1353.
[17] G. Zotti, G. Schiavan, S. Zecchin, J. Electrochem. Soc. 145 (1998) 385–389.
[18] R. Schrebler, K. Bello, F. Vera, P. Cury, E. Munoz, R. Rio, H.G. Meier, R. Cordova, E.A. Dalchiele, Electrochem. Solid-State Lett. 9 (2006) C110–C113.
[19] C. Pascal, J.L. Pascal, F. Favier, Chem. Mater. 11 (1999) 141–147.
[20] T. Fujii, F.M.F. de Groot, G.A. Sawatzky, Phys. Rev. B 59 (4) (1999) 3195–3202.
[21] N.S. McIntyre, D.G. Zetaruk, Anal. Chem. 49 (11) (1977) 1521–1529.
[22] Xian-Ming Liu, Shao-Yun Fu, Hong-Mei Xiao, J. Solid State Chem. 179 (2006) 1554–1558.
[23] Y. Ni, X. Ge, Z. Zhang, Q. Ye, Chem. Mater. 14 (2002) 1048–1052.
[24] K.I. Popov, M.G. Pavlovic, in: R.E. White, B.E. Conway, J.O'M. Bockris (Eds.), Modern aspects of electrochemistry, 24, Plenum Press, New York, 1993, pp. 299–391.
[25] I. Banerjee, Y.B. Khollam, C. Balasubramanian, R. Pasricha, P.P. Bakare, K.R. Patil, A.K. Das, S.V. Bhoraskar, Scripta Mater. 54 (2006) 1235–1240.
[26] Sushil Raj Kanel, Jean-Mark Greneche, Heechul Choi, Environ. Sci. Technol. 40 (2006) 2045–2050.